Design and Simulation of Ring Resonator Optical Switches using Electro-Optic Materials

Yuichiro TANUSHI* and Shin YOKOYAMA

Research Center for Nanodevices and Systems, Hiroshima University, 1-4-2 Kagamiyama, Higashi-Hiroshima, Hiroshima 739-8527, Japan

Ring resonator optical switches using electro-optic materials have been proposed. The propagation loss of the waveguides and the resonance characteristics of ring resonators with different refractive indices are simulated. The operation voltage is estimated based on the results of the simulations and is found to be 0.70 V in the case of the ring resonator switch with a K(Ta, Nb)O$_3$ core and KH$_2$PO$_4$ cladding layers. The time-dependent resonance characteristics are calculated by a simple model. The operation speed is limited by the resonance time and is less than 15 ps. This is different from optical switches with a Si core, where their operation speed is limited by not the resonance time but the free carrier accumulation time of the order of 10^2 ps. Ring resonator switches with electro-optic materials are promising devices for application to optically interconnected LSIs because of their size of around 20 μm and high operation frequency of more than 66 GHz.   [DOI: 10.1143/JJAP.45.3493]

KEYWORDS: ring resonator, optical switch, electro-optic material, optical interconnection, monolithic integration, FDTD simulation

1. Introduction

Optical interconnection on Si chips is an attractive candidate for solving the signal delay of metal interconnections.[1] Si-based light-emitting devices are desirable for integration, however light-emitting devices are the most difficult devices to fabricate with Si technology. Although many studies have been carried out to create Si-compatible light-emitting materials, for example, Er-doped crystalline Si[2] and β-FeSi$_2$,[3] practical Si-based light-emitting devices have not been realized yet. Therefore, it is unavoidable to use light-emitting devices made of compound semiconductors. However, it is not easy to integrate such devices on Si chips. We believe that a more promising method is to integrate optical switches monolithically. We are studying the use of tunable microring resonators for optical switches because of their compactness.[4] It has also been shown that microring resonators are an attractive candidate for small optical filters.[5]

To realize tunable ring resonators, it is necessary to control the refractive index of the waveguide by using an external field. Tunable polymer ring resonators with the thermo-optic effects have been fabricated,[6] but their response time is slow (∼5 ms). Recently, Almeida *et al.* fabricated ring resonator Si switches using optical control signals and reported a fast operation speed of 450 ps.[7] However, all-optical switches cannot be used in the optical interconnection in LSI. In order to realize fast ring resonator switches for optical interconnection, a waveguide whose refractive index is changed by an electric field is needed. There are two solutions to realizing such a waveguide: electro-optic (EO)-material-core waveguide and Si-core waveguide.[8] We focus on EO materials because faster operation can be expected. In this study, ring resonator switches are designed and their operation voltage and speed are estimated.

2. Operation Voltage

A ring resonator switch consists of a ring and input/output (I/O) waveguides, as shown in Fig. 1(a). Resonance wavelengths of this device are given by
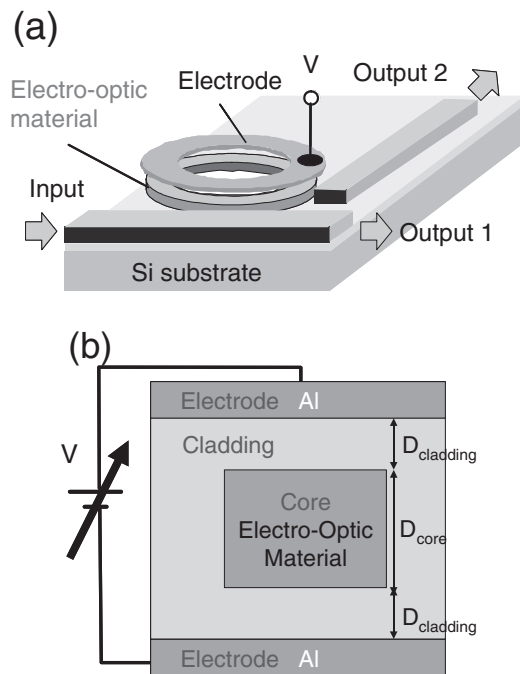

(a)

(b)

Fig. 1. (a) Ring resonator optical switches with electro-optic materials and (b) cross-sectional structure of the ring waveguide. In the simulation, the ring radius and waveguide width are fixed at 12 and 2 μm, respectively.

$$\lambda = \frac{n_{eq} \cdot 2\pi R}{m_\lambda}, \qquad (1)$$

where n_{eq} is the equivalent index of the waveguide, R is the ring radius, and m_λ is an arbitrary integer. Figure 1(b) shows the cross-sectional structure of the ring waveguide, which consists of an EO-material core layer, cladding layer, and aluminum electrodes. D_{core} and $D_{cladding}$ denote the thicknesses of the core and the cladding layer, respectively. We choose LiNbO$_3$ (LN), (Ba, Sr)TiO$_3$ (BST), and K(Ta, Nb)O$_3$ (KTN) as the core materials. LN is a widely used EO material, but has not yet been introduced in the Si process. BST has already been introduced in the Si process as the ferroelectric material of memory devices.[9] KTN was recently developed by NTT Photonics Laboratories[10] and

*E-mail address: tanushi@sxsys.hiroshima-u.ac.jp

Table I. Refractive index, EO coefficient, and dielectric constant of three kinds of EO materials. The operation voltages for ring resonator switches with these materials calculated using eq. (2) are also listed. The first and second values of the operation voltage are for SiO_2 and KH_2PO_4 being used as the cladding layer, respectively. Both materials have a low refractive index (1.46 for SiO_2 and 1.47 for KH_2PO_4), and thus are effective as the cladding layer.

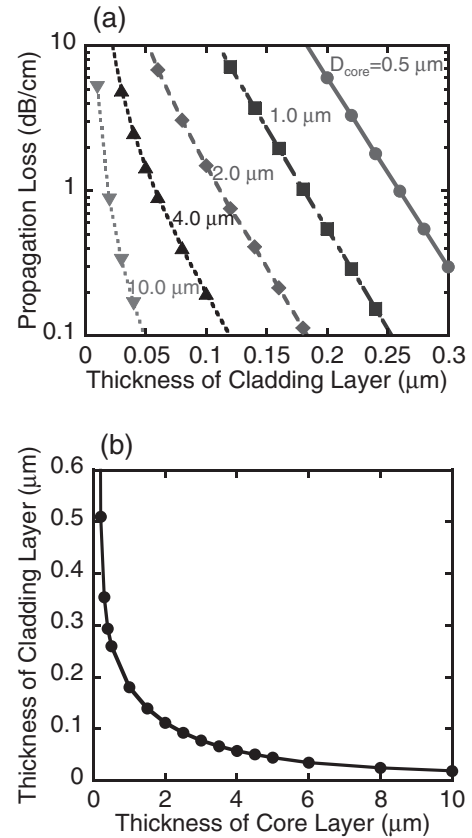|	$LiNbO_3$	(Ba, Sr)TiO_3	K(Ta, Nb)O_3
Refractive index	2.2	2.1	2.35
EO coefficient (pm/V)	30.8	23	600
Dielectric constant	28	300	666
Operation voltage (V)	10.7/2.36	56.9/17.5	2.12/0.70

Fig. 2. (a) Simulated dependence of propagation loss on the thicknesses of core and cladding layers, by finite difference method. (b) Relationship between the thickness of core layer and that of cladding layer for propagation loss of less than 1.0 dB/cm. The core and cladding materials are LN and SiO_2, respectively.
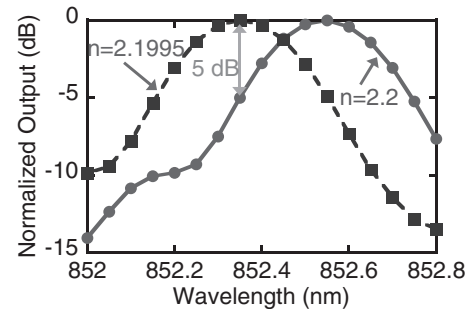

Fig. 3. Simulated resonance properties for different refractive indices of the core, by 2D FDTD method. Output power is normalized by peak power. Refractive index change of 5×10^{-4} is needed for switching operation with switching gain of 5 dB at $\lambda = 852.35$ nm. The subpeak at $\lambda = 852.15$ nm may be a resonance from a higher mode because the ring waveguide has multimodes.

it has a very large EO coefficient. The refractive indices, EO coefficients, and dielectric constants of the above materials are summarized in Table I. For the cladding layer, SiO_2 or KH_2PO_4 (KDP) is adopted. KDP has a low refractive index of 1.47 and high dielectric constant of 42. Therefore, low-voltage operation is expected, as explained in the following calculations.

Optical properties were simulated to estimate operation voltage, using the optical simulator, Appolo Photonics Solutions Suite. In these simulations, ring radius and waveguide width were fixed at 12 and 2 μm, respectively. To determine the thickness of the core and the cladding layers, the propagation loss was simulated by the finite difference method at the wavelength of a GaAs laser diode (850 nm). The simulation was performed in the transverse electric (TE) mode because the propagation loss of the TE mode is less than that of the transverse magnetic (TM) mode. Figure 2(a) shows the dependence of the propagation loss on the thickness of the cladding layer for several thicknesses of the core layer. This propagation loss is caused by absorption due to the aluminum electrode. If the core layer is thin, the confinement of the field becomes poor; therefore, a thick cladding layer is necessary. The thickness of the cladding layer required to reduce the propagation loss to less than 1.0 dB/cm is shown in Fig. 2(b). In this simulation, we assumed the core and cladding materials to be LN and SiO_2, respectively. The results do not change considerably for other core and cladding materials because they have similar refractive indices (see Table I).

Then resonance properties of the ring resonator are simulated by the two-dimensional finite difference time domain (2D FDTD) method, as shown in Fig. 3. The ring radius and the gap between the ring and I/O waveguides are fixed at 12 and 0.1 μm, respectively. Propagation loss due to the aluminum electrode is included in the complex equivalent index. The 2D FDTD simulation is less accurate than the 3D FDTD simulation and insufficient to predict the resonance wavelength of the ring resonator precisely. However, the 2D FDTD method is satisfactory for estimating the shift of the resonance wavelength. Output power is normalized by peak power. A refractive index change Δn of 5×10^{-4} is needed for switching operation with the switching gain of 5 dB at $\lambda = 852.35$ nm. This refractive index change causes the resonance peak shift of 0.2 nm, which is consistent with eq. (1).

From the above numerical results, the operation voltage is estimated. Operation voltage V depends on the thickness D

and the dielectric constant ϵ of the core and cladding materials as

$$V = \left(D_{core} + 2 \frac{\epsilon_{core}}{\epsilon_{cladding}} D_{cladding} \right) E, \qquad (2)$$

where E is the electric field applied to the core layer to change its refractive index Δn and is expressed as a function of the refractive index n and EO coefficient r of the core material,
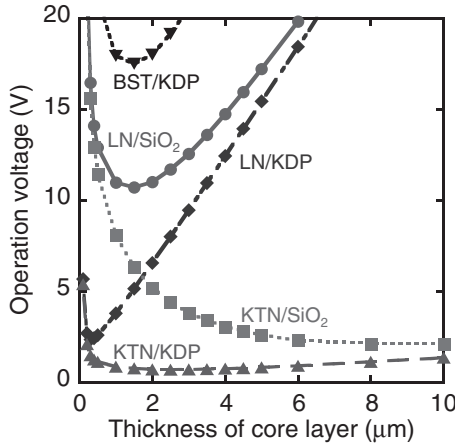
Fig. 4. Dependence of operation voltage on the core thickness for various combinations of core and cladding materials. The cladding layer thickness is chosen such that the propagation loss becomes less than 1.0 dB/cm. Operation voltage for the KTN/SiO$_2$ combination does not have a minimum value, however it is saturated for a thick core layer.

$$E = -\frac{2}{n^3 r} \Delta n. \tag{3}$$

Figure 4 shows the dependence of the operation voltage on the thickness of the core layer for several combinations of core (LN, BST, and KTN) and cladding (SiO$_2$ and KDP) materials. The thickness of the cladding layer for a given core layer thickness is selected as shown in Fig. 2(b). The operation voltage for the KTN/SiO$_2$ combination does not have a minimum value, however, it is saturated for a thick core layer. Therefore, the operation voltage is estimated at $D_{\mathrm{core}} = 10\,\mu$m. The minimum operation voltage for the BST/SiO$_2$ combination is 56.9 V at $D_{\mathrm{core}} = 6\,\mu$m, and is not shown in this figure.

The results are summarized in Table I. In this estimation, a single-crystal thin film is assumed, therefore, if the thin film is polycrystalline or amorphous, the operation voltage becomes higher. KTN is promising if a thin crystal film is available in the Si process, particularly when using KDP as the cladding layer. LN and BST have higher operation voltages. These values may be reduced by introducing other waveguide structures, such as a ridge type, where the entire electric field can be effectively applied to the core material.

3. Operation Speed

The operation speed is estimated using a simple model, as shown in Fig. 5. This model has a time-dependent analytic solution and therefore is suitable for estimating the operation speed. The simulation results given in the previous section are not used in this section. This model neglects waveguide width and assumes an equivalent index. We fix the equivalent index at 2.0 for EO material. The other model parameters are the coupling constant between the ring and I/O waveguides $\sin(\kappa)$, and the bending loss of the ring denoted by the absorption coefficient α. In this model, the output spectrum when the light propagates for m rounds in the ring $T_m(\lambda)$ is calculated as

$$T_m(\lambda) = \frac{Y^2[1 + X^{2m} - 2X^m \cos(m\phi(\lambda))]}{1 + X^2 - 2X \cos\phi(\lambda)}, \tag{4}$$
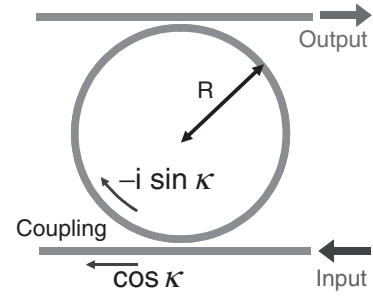

Fig. 5. Simple model of the ring resonator. Waveguide width is neglected and an equivalent index is assumed. The ring and I/O waveguide are coupled with the coupling constant $\sin(\kappa)$. The bending loss of the ring is denoted by the absorption coefficient α.

where X, Y, and $\phi(\lambda)$ are the same as in ref. 11 and are given by

$$X = \cos^2(\kappa) \exp(-\alpha \cdot \pi R), \tag{5}$$

$$Y = \sin^2(\kappa) \exp(-\alpha \cdot \pi R/2), \tag{6}$$

$$\phi(\lambda) = n_{\mathrm{eq}} \frac{4\pi^2 R}{\lambda}. \tag{7}$$

The resonance characteristics at a sufficiently long time to reach stable response are obtained in the limit of $m \to \infty$ in eq. (4). In this limit, X^{2m} and X^m vanish, thus $T_m(\lambda)$ is reduced to eq. (1) in ref. 11:

$$T_\infty(\lambda) = \frac{Y^2}{1 + X^2 - 2X \cos\phi(\lambda)}. \tag{8}$$

We calculated the dependence of resonance characteristics on the coupling constant and the bending loss using eq. (8) to determine suitable device parameters. Figures 6(a) and 6(b) show the coupling constant $\sin(\kappa)$ dependences of the resonance peak power and the full width at half maximum (FWHM) of the resonance shape, respectively, at several bending losses per round, $\exp(-\alpha \cdot 2\pi R)$. Weaker coupling results in lower peak power and narrower resonance width (higher Q-factor). The FWHM should be less than 0.2 nm for optical switching operation with switching gain of 5 dB (see Fig. 3), therefore, the coupling constant must be smaller than 0.3. On the other hand, the coupling constant should be larger than 0.1 to achieve a practical strong output, as shown in Fig. 6(a). Large bending loss results in smaller peak power and wider FWHM; thus a small bending loss is better. According to Fig. 6(b), the bending loss must be smaller than 1 dB/round. In the following calculation, the coupling constant is fixed at 0.2 and the bending loss remains free parameter.

Figure 7(a) shows an example of the resonance shape for a coupling constant of 0.2 after light propagates in the ring for 5, 30, and 100 rounds. It takes 0.5 ps to propagate one round in the ring. After 100 rounds, the resonance shape almost reaches the final shape. For comparison, the resonance shape for a coupling constant of 0.3 is also shown in Fig. 7(b). In this case, 30 rounds is sufficient for stabilization of the resonance shape. Time dependences of peak power and FWHM are shown in Figs. 8(a) and 8(b), respectively. FWHM reaches 0.2 nm within 15 ps, except when bending loss is large (>1 dB/round). Thus resonance
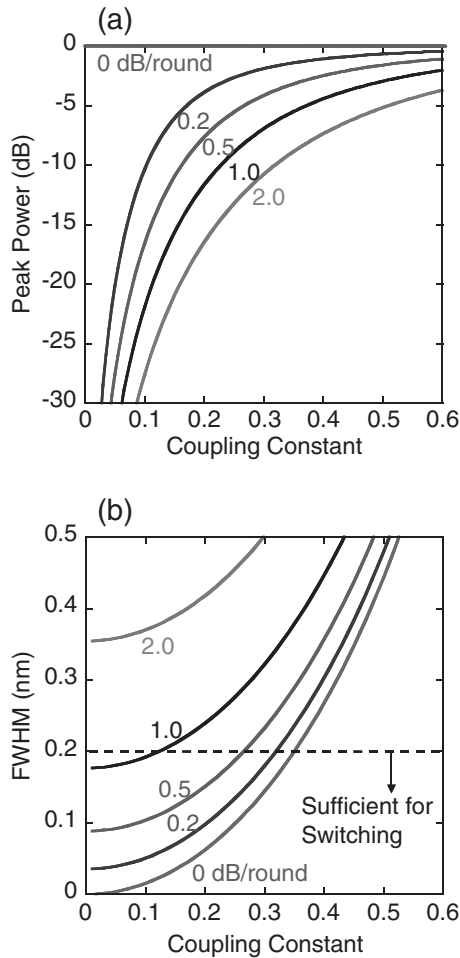
Fig. 6. Dependence of (a) resonance peak power and (b) FWHM of the resonance shape on the coupling constant and the bending loss per round. Weaker coupling results in lower peak power and narrower resonance width. With increasing bending loss, the peak power decreases, particularly for a small coupling constant, and the FWHM increases.

time is estimated to be 15 ps. This value is supported by another estimation using the Q-factor. The Q-factor of the ring resonator for a coupling constant of 0.2 with no bending loss is 13900. The Q-factor is related to the lifetime of the field energy accumulated in the ring τ[12]

$$Q = \frac{2\pi c \tau}{\lambda}. \qquad (9)$$

Therefore, the field energy lifetime is estimated to be 6.3 ps.

The operation speed of the ring resonator switches using EO materials depends on not only resonance time but also the RC delay and polarization times of the EO materials for refractive index change. We roughly estimated the RC delay time by assuming a parallel-plate capacitor. The cross-sectional structure of the capacitor is as shown in Fig. 1(b). The length of the capacitor is the circumference of the ring, $2\pi R = 75.4\,\mu m$, and the width and thickness of the aluminum electrode are 3.4 and 0.8 μm, respectively. In this estimation, the RC delay time is about 10^{-2} ps for any combination of the three kinds of EO materials, LN, BST, and KTN, and cladding materials, SiO_2 and KDP. The polarization time of EO materials is less than 10 ps because Ti-diffused $LiNbO_3$ optical modulators are reported to operate at over 100 GHz.[13] The RC delay time and the
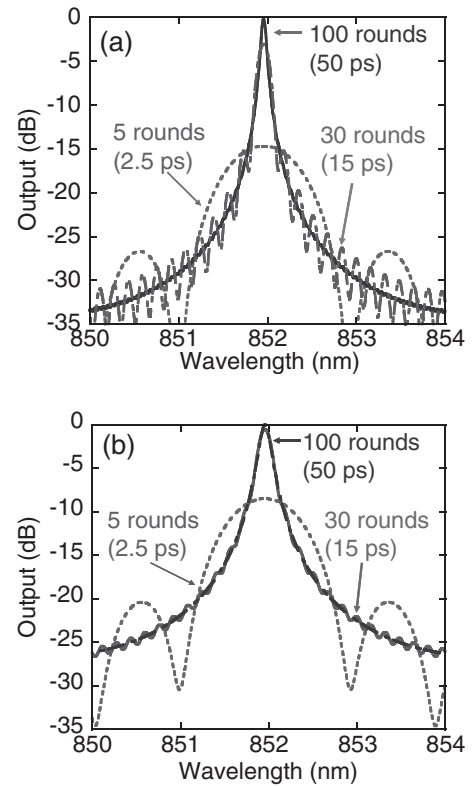

Fig. 7. Time dependence of resonance characteristics for coupling constant of (a) 0.2 and (b) 0.3. In both cases, no bending loss is assumed.
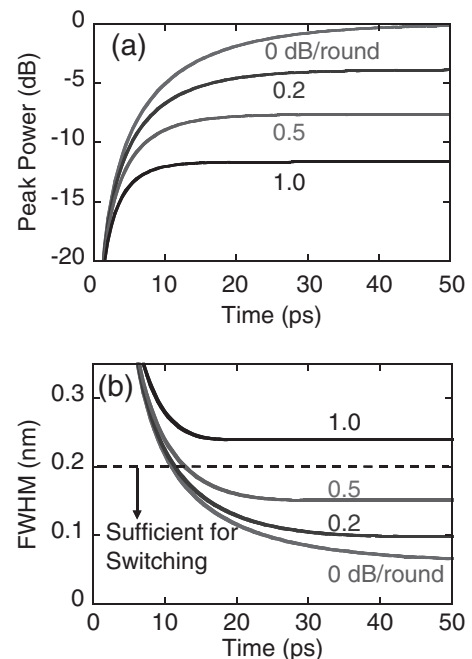

Fig. 8. Time dependence of (a) peak power and (b) FWHM for coupling constant of 0.2. It takes less than 15 ps to reach FWHM of 0.2 nm when bending loss is sufficiently small.

polarization time are shorter than the resonance time (~15 ps), therefore, the operation speed is limited by the resonance time, and the operation frequency is estimated to be more than 66 GHz. This is different from optical switches using a Si core,[8] where the operation speed is limited by not
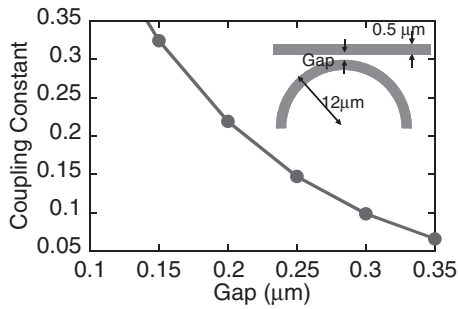
Fig. 9.   2D FDTD simulation of coupling constant in TE mode.

resonance time but free carrier accumulation time for a refractive index change of the order of 10^2 ps.

Next, the gap dependence of the coupling constant between ring and I/O waveguides in the TE mode is simulated by the 2D FDTD method at $\lambda = 850$ nm. Here, the material filled in the gap is SiO_2. Device dimensions and simulated results are shown in Fig. 9. In this simulation, we set the waveguide width at 0.5 μm for a single-mode channel waveguide. The coupling constant of 0.2 is obtained from the gap of 0.21 μm. This gap size is feasible in a conventional Si process.

4.   Conclusions

We proposed ring resonator optical switches using EO materials. The propagation loss of the channel waveguides with EO materials and the shift of the resonance wavelength due to the change of the refractive index of the core layer were simulated. The operation voltage was estimated on the basis of the results of the simulations and was 0.70 V in the case of a KTN core and KDP cladding layers. In other cases, the operation voltage was relatively high. Waveguides with different structures, such as the ridge type, are needed to reduce the operation voltage. We calculated the time

dependence of the resonance characteristics by a simple model and showed that the operation speed is limited by not the RC delay and polarization times but the resonance time. In this model, the operation time was estimated to be shorter than 15 ps. The ring resonator switches with EO materials are promising devices for application to optically interconnected LSI because of their size and fast operation speed.

1) I. Hayashi: Jpn. J. Appl. Phys. **32** (1993) 266.
2) G. Franzo, S. Coffa, F. Priolo and C. Spinella: J. Appl. Phys. **81** (1997) 2784.
3) T. Suemasu, K. Takakura, C. Li, Y. Ozawa, Y. Kumagai and F. Hasegawa: Thin Solid Films **461** (2004) 209.
4) Y. Tanushi, M. Wake, K. Wakushima, M. Suzuki and S. Yokoyama: Proc. 1st Int. Conf. Group IV Photonics, Hong Kong, 2004, WB3.
5) B. E. Little, S. T. Chu, H. A. Haus, J. Foresi and J.-P. Laine: J. Lightwave Technol. **15** (1997) 998.
6) Y. Yanagase, S. Yamagata and Y. Kokubun: Electron. Lett. **39** (2003) 922.
7) V. R. Almeida, C. A. Barrios, R. R. Panepucci and M. Lipson: Nature **431** (2004) 1081.
8) A. Liu, R. Jones, L. Liao, D. Samara-Rubio, D. Rubin, O. Cohen, R. Nicolaescu and M. Paniccia: Nature **427** (2004) 615.
9) W. Fan, B. Kabius, J. M. Hiller, S. Saha, J. A. Carlisle, O. Auciello, R. P. H. Chang and R. Ramesh: J. Appl. Phys. **94** (2003) 6192.
10) S. Toyoda, K. Fujiura, M. Sasaura, K. Enbutsu, A. Tate, M. Shimokozono, H. Fushimi, T. Imai, K. Manabe, T. Matsuura, T. Kurihara, S. C. J. Lee and H. de Waardt: Electron. Lett. **40** (2004) 830.
11) Y. Kokubun: Oyo Buturi **72** (2003) 1364 [in Japanese].
12) A. Yariv: *Optical Electronics in Modern Communications* (Oxford Univ. Press, Oxford, 1997) 5th ed., Chap. 4.
13) K. Noguchi, O. Mitomi and H. Miyazawa: J. Lighwave Technol. **16** (1998) 615.